Proceedings of ASME Turbo Expo 2011
GT2011
June 6-10, 2011, Vancouver, British Columbia, Canada

GT2011-45674

THE EFFECTS OF IMPROVED STARTING CAPABILITY ON ENERGY YIELD FOR SMALL HAWTS

Supakit Worasinchai
School of Engineering
and Computing Sciences
Durham University
South Road, Durham DH1 3LE
Email: supakit.worasinchai@durham.ac.uk

Grant Ingram*
School of Engineering
and Computing Sciences
Durham University
South Road, Durham DH1 3LE
Email: g.l.ingram@durham.ac.uk

Robert Dominy
School of Engineering
and Computing Sciences
Durham University
South Road, Durham DH1 3LE
Email: r.g.dominy@durham.ac.uk

ABSTRACT

The purpose of this study was to investigate the effect of turbine starting capability on overall energy-production capacity. The investigation was performed through the development and validation of MATLAB/Simulink models of turbines. A novel aspect of this paper is that the effects of load types, namely resistive heating, battery charging, and grid connection were also investigated.

It was shown that major contributors to improved starting performance are aerodynamic improvements, reduction of inertia, and simply changing the pitch angle of the blades. The first two contributors can be attained from an exploitation of a "mixed-aerofoil" blade.

The results indicate that starting ability has a direct effect on the duration that the turbine can operate and consequently its overall energy output. The overall behaviour of the wind turbine system depends on the load type, these impose different torque characteristics for the turbine to overcome and lead to different power production characteristics.

When a "mixed-aerofoil" blade is used the annual energy production of the wind systems increases with the exception of resistive heating loads. Net changes in annual energy production were range of -4% to 40% depending on the load types and sites considered.

The significant improvement in energy production strongly suggests that both the starting performance and load types should be considered together in the design process.

NOMENCLATURE

A Aerofoil cross-section area
c Scale factor
C_P Power coefficient
F Weibull distribution
I Current
J Moment of inertia
k Shape factor
K Generator constant
MX Mixed-aerofoil blade
MP Mixed-aerofoil blade with pitch
P Power
R Load resistance
r Radius
SG Single-aerofoil blade
T Torque
U Wind speed
V Voltage
α Rotor acceleration
Γ Gamma function
λ Tip speed ratio
ω Rotor speed
ρ Air density
θ_P Pitch angle

*Address all correspondence to this author.

INTRODUCTION

It is estimated that small wind systems can play a significant role in energy production [1] and the use of small-scale wind turbines to produce power has become increasingly popular. However, it is well-known that these small devices normally operate in relatively unsteady and low-wind conditions and, as a consequence, their ability to produce useful power is still in question.

These small turbines often employ a fixed-pitch and single-aerofoil blade configuration to promote simplicity in design and manufacturing. This configuration makes them operate with a wider incidence angle range, leading to significantly different operational characteristics in comparison to large-scale machines.

Unlike vertical-axis machines for which the starting process remains problematic and poorly understood, small horizontal axis wind turbines (HAWTs) can self-start and generate useful power once the cut-in speed has been achieved. The design of these small systems, as a consequence, has focused on their peak power-extraction performance [2,3] and their starting capabilities seem to be largely overlooked.

The study of starting performance of small HAWTs is relatively immature and little useful information is available in the literature. Some papers have focused on the starting behaviour [4–6] and others focused on the design of blades with better starting performance [7–9].

Experiments on small HAWTs have revealed some important starting characteristics. An experiment on a two-bladed 5kW turbine by Ebert and Wood [4] showed that there are two main processes taking place in the starting sequence, namely periods of idling and rapid acceleration. During the idling period, the turbine blade rotates with slow acceleration and the angle of attack gradually decreases until the blade can generate a high lift-to-drag ratio. Here the turbine enters its rapid acceleration phase with the blades continuing to accelerate more rapidly to the point at which useful power can be extracted. These two periods complete the whole starting sequence. It was also noted that the acceleration period is comparatively short and can be ignored in terms of designing a turbine for improved starting performance. This long idling period was a direct result of the high angle of attack that the blade was initially exposed to.

Mayer, et al. [5] researched experimentally the effect of blade pitch angle (θ_P) on the idling period through pitch angle variations from 0° to 35° with a 5° increment. They found that, with increased pitch angle, the idling period was shortened due to the lower angles of attack that the blade experienced.

Wright and Wood [6] further investigated the starting performance of a small HAWT. A three-bladed, 2m diameter turbine was experimentally investigated and the authors confirmed that the torque generated near the hub plays a particularly important role in spinning the rotor up to speed while torque at the tip plays a more significant role in power production.

The finding from Wright and Wood's experiment led to the design of rotors having good starting and power-extraction performance [7–9]. An evolutionary algorithm was employed by Hampsey [7] to design an improved turbine blade and he found that his newly-designed blade had better starting performance and could accelerate more quickly than conventional designs while still giving good peak power output. The main contribution to this improvement was from a reduction in the moment of inertia. Hampsey's method was further improved by Wood [8] and Clifton-Smith and Wood [9] to design new rotors that provide a good compromise between starting torque and power extraction. They found that the best power-extraction blades always had relatively poor starting performance and a long idling period due to a high angle of attack along the blade but it was possible to design blades that suffered a small reduction in power production but improved start-up time.

Even though the starting sequence has been investigated under turbulent wind by a number of researchers [4–6], until this paper load types that influence the overall turbine performance have not been considered.

Although aerofoil families have been designed to enhance rotor performance [10,11], it is common for small HAWT blades to be designed using a single aerofoil profile which is scaled over the blade span (single-aerofoil blade) [12,13]. The mixed-aerofoil blade (employing different aerofoil shapes in different blade sections) is normally used in preference to the single-aerofoil blade due to the fact that the aerofoils at different sections are exposed to different flow conditions and requirements. Although the mixed-aerofoil blade design is well established, it is generally adopted to maximise energy capture performance, and more specifically, optimised to operate within a narrow range of Reynolds numbers and angles of attack. The exploitation of a mixed-aerofoil blade for self-starting improvement has not been investigated in detail, not least because of the lack of aerofoil data at low Reynolds number and high angles of attack.

The purpose of this work is twofold.

1. To investigate the impact of employing a mixed-aerofoil blade to improve starting capability by comparison of different blades designs
2. To estimate the impact load types have when attempts are made to improve the starting performance of small HAWTs

MODELLING ASSUMPTIONS

ROTORS

The starting capability of a turbine (or rotor acceleration, α) can be mathematically expressed as

$$\alpha = \frac{T_a - T_r}{J} \tag{1}$$

where T_a is aerodynamic torque generated by the rotor, T_r is resistive torque generated by other components, and J is the rotor inertia. It can be seen that, with constant resistive torque, the acceleration can be improved by increasing aerodynamic torque and decreasing rotor moment of inertia.

Aerodynamic torque generated by the rotor depends on many factors such as the aerofoil used and the pitch angle. There are a number of ways of generating higher starting torque. Increasing the the number of blades is one option but the disadvantage is that it also introduces additional inertia to the rotor. A further disadvantage is that the higher number of blades (or solidity) produces a narrow power curve with a sharp peak resulting in a turbine which is very sensitive to changes in tip speed ratio [14], a configuration that is clearly not suitable for small turbines operating in turbulent areas.

It was also shown by Mayer et al. [5] that, by increasing the pitch angle, the blade would generate more torque as the blade experiences a smaller angle of attack. This also reduces the idling as the blade produces a higher lift-to-drag ratio. However, with the increase in pitch angle the turbine performance curve is shifted towards a lower tip speed ratio and so the turbine will stall earlier resulting in unsatisfactory performance at higher wind.

The second factor involved in starting is rotor inertia which is related to the blade geometry and material used as follows:

$$J = \rho \sum_{i}^{n} A_i r_i^2 \Delta r_i \tag{2}$$

where ρ is density of material used, r is radius, and A is cross-section area of blade at the radius r. It can be seen that, apart from the material used, the inertia is directly related to the blade size. The size of the rotor is determined by the chord distribution and aerofoil shape. The chord distribution is normally designed using established design procedures from the aerofoil chosen [14]. It is, therefore, reasonable to conclude that obtaining an inertia reduction is dependant on the aerofoil employed.

From these considerations, the starting capability can be improved through a careful selection of an aerofoil that exhibits high lift-to-drag ratio and has a small cross-sectional area. However, an aerofoil with a small cross-section (or thin aerofoil) is unlikely to be suitable for the root section that experiences a high bending moment. It is therefore common to employ an aerofoil with an acceptable compromise between optimal structural and aerodynamic requirements in which the same section will be employed all along the blade albeit with changing twist and chord (a "single-aerofoil" blade) [12, 13].

This raises the question as to whether it is beneficial to employ a "mixed-aerofoil" blade in which the blade profile changes along its span. Suitable aerofoils would be selected to generate high torque without introducing additional inertia or sacrificing the power-extraction performance at high wind speeds.

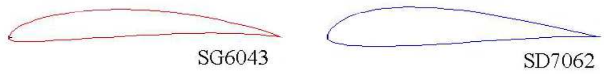

FIGURE 1. AEROFOILS.

It should be noted that the use of mixed-aerofoil blades is not new and various series of aerofoil profiles (also called aerofoil families) have been designed for different blade sections e.g. [10, 11]. However, their impact on self-starting had not been investigated to date. An accurate estimation of their self-starting performance can only be completed if aerodynamic data is available at suitable Reynolds numbers and high angles of attack. This aerodynamic data is scarce and not readily available in the literature.

In this new study, numerical investigations of aerofoil performance using an unsteady two dimensional Reynolds Averaged Navier Stokes (RANS) solver were performed to select promising aerofoils. The key requirement was that aerofoils should exhibit a high lift-to-drag ratio at low Reynolds number. Two promising aerofoils emerged, the SG6043 [15] and SD7062 [16], proposed by Selig. The profiles are depicted in Figure 1.

The SG6043 was designed by Selig and Giguere for small wind turbine applications. Its thickness and camber are 10% and 5.5%, respectively and it has a high lift-to-drag ratio. The SD7062 was designed for gliders by Selig and Donovan at the University of Illinois. It exhibits high lift and low drag at low speed. It has a thickness of 14% and camber of 4%. This aerofoil is thicker than the SG6043 and can be employed for root sections.

These aerofoils have been tested experimentally at low Reynolds numbers and through 360° of angle of attack (conditions which small turbines experience at startup) at Durham University. An example of lift and drag coefficients of the SG6043 at a nominal Reynolds number of 90,000 through 360° is shown in Figure 2. More details of this work can be found in Worasinchai et al [17]. A novel aspect of this paper is that this is the first startup simulation conducted with aerofoil data obtained at correct Reynolds numbers and incidence angle.

Based upon these aerofoil data, three alternative simulated blades have been defined and their relative performance is presented here. The first simulated blade was a single-aerofoil design based upon the SD7062 aerofoil over the full span and was designed to produce 1kW at a rotational speed of 700RPM and a wind speed of 10 m/s. The blade was designed using the method described by Burton et al [14]. This blade was set at a pitch angle of 5° and is referred to as the *SG* blade in this paper.

The second simulated blade was a mixed-aerofoil blade which was obtained by replacing the outer two-thirds of the span with the SG6043 aerofoil. The intent was to produce a high aero-

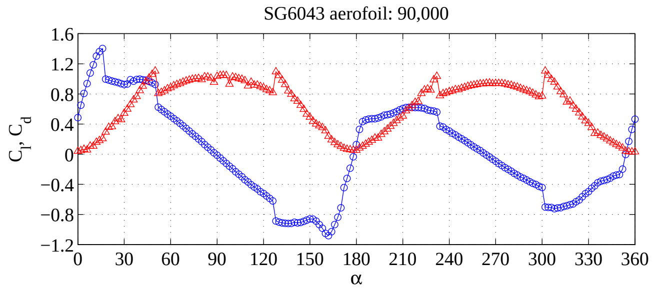

FIGURE 2. THE SG6043 PERFORMANCE CHARACTERISTICS.

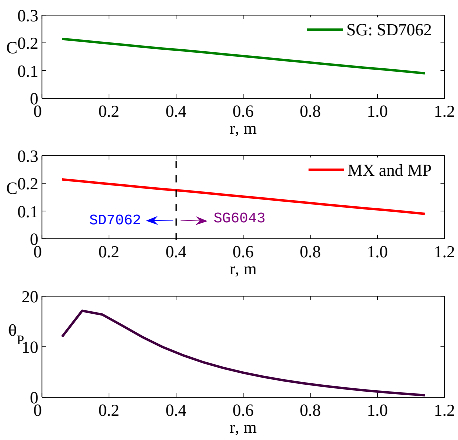

FIGURE 3. BLADE GEOMETRIES.

dynamic torque with a smaller cross-sectional area contributing to a lower inertia whilst retaining the SD7062 profile at the blade root. This blade is referred to as the *MX* blade in this paper.

The third blade was designed to further improve starting performance of the mixed-aerofoil blade by increasing the pitch angle to 6° to reduce high angles of attack at start-up. This design is labelled as *MP* in this paper.

Rotor inertias were calculated using equation 2 and it was found that the mixed-aerofoil rotor exhibited a 21-percent reduction in moment of inertia relative to the SD7062-based single-aerofoil design (see Table 1).

TABLE 1. DESIGN PARAMETERS.

Parameter	SG	MX	MP
Rated power (W)	1,000	1,000	1,000
Rated speed (RPM)	700	700	700
Rated wind (m/s)	10	10	10
Radius (m)	1.2	1.2	1.2
Aerofoil	SD7062	SD7062 + SG6043	SD7062 + SG6043
Inertia ($kg-m^3$)	2.5668	2.0287	2.0287
Pitch angle (degree)	5°	5°	6°

TABLE 2. RESISTIVE TORQUES.

Resistive torque	Value (Nm)
Cogging torque (stationary)	0.45
Cogging torque (rotating)	0.30
Load resistive torque	load-dependent

GENERATORS AND LOAD TYPES

Small wind turbines are most commonly coupled to permanent magnet generators [18, 19] and this study assumes the use of such generators although the analysis is easily extended to include other generator characteristics if required.

One of the inherent properties of these generators is their cogging torque that has to be overcome by the turbine. Even though recent research has shown that permanent magnet generators can be designed with no cogging torque [19], it seems reasonable to consider this cogging torque in this analysis as it remains relevant to many currently used systems.

The cogging torque created by permanent magnet generators depends on many factors such as rated size and configuration [18] and methods of calculating this cogging torque are available [20,21]. However, detailed analysis is beyond the scope of this study and a simple estimation has been used. It has been reported that typical cogging torques of permanent magnet generators rated from 500W to 1.5kW are 0.3 to 0.6 Nm, respectively [22]. Since the turbine considered here is a 1kW device, a cogging torque of 0.45 Nm is assumed.

In addition to the cogging torque that acts when starting from rest, the generator also adds a resistive torque when rotating. In the Wright and Wood experiment [6] in which a 600W rated generator was considered, a constant resistive torque of 0.24 Nm was applied when the generator was moving. Since a larger generator is considered here, a resistive torque of 0.3 Nm was used in this study. Table 2 summarises all resistive torques used in this paper's calculation.

Small turbines are usually used for stand-alone applications including battery charging and resistive heating. Nevertheless, it is also possible to employ these small turbines to generate power to the grid through a grid-tie converter [23]. Load types considered in this paper are battery charging, resistive heating, and grid connection, each having different characteristics. Mathematical descriptions of these loads were obtained through the analysis of equivalent circuits. Detailed derivations and validations of these equations can be found in Stannard [23]. Figure 4 presents a schematic diagram of these three different loads together with

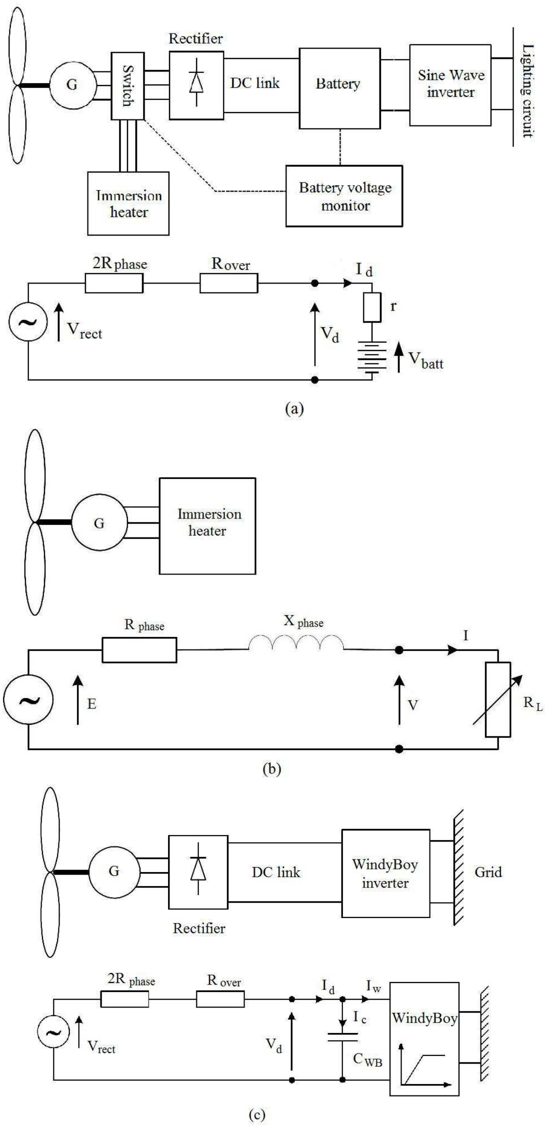

FIGURE 4. SCHEMATIC DIAGRAMS AND EQUIVALENT CIRCUITS: (a) BATTERY CHARGING (b) RESISTIVE HEATING (c) GRID CONNECTION.

their corresponding equivalent circuits.

WIND MODELS

Both real and simulated wind data are used in this paper. The wind data used was measured in East Kilbride, Glasgow by NaREC (National Renewable Energy Centre) covering the period from 15 May 2008 to 2 July 2009 [24]. The wind data were averaged over a five-minute interval. One-minute data is also available from 15 May 2008 to 15 June 2008. It is important to note that the real wind data has a temporal resolution of minutes but that the starting behaviour of a turbine occurs over a much smaller time scale, typically seconds. In addition the real wind data is site-specific.

A turbulent wind model simulator which was developed by Stannard [23] was employed in this simulation in addition to the real wind data as it provides the temporal resolution required (in a scale of seconds) and allows estimation of site variations.

MATLAB/SIMULINK IMPLEMENTATION

The aforementioned models (rotors, loads, and turbulent wind) were individually modelled using the MATLAB/SIMULINK environment. Blade element momentum (BEM) theory was employed to estimate aerodynamic torque. Load models (battery, resistive heating, and the grid) were modelled using subsystem blocks provided by SIMULINK. The implementation of this model was based on the assumption that the system can be considered quasi-steady.

In essence, starting behaviour of the turbine is modelled using a time-stepping approach. The rotational speed of the rotor at the next time step can be mathematically expressed as:

$$\omega_{n+1} = \omega_n + \left(\frac{T_{a,n} - T_{r,n}}{J}\right)\Delta t_n \tag{3}$$

where ω is turbine rotational speed and Δt is time step used in the simulation. A variable-step was used to adjust the time as the speed changed.

The resistive torque caused by different loads is computed using the following equations:

Resistive load:

$$T_{r,n} = \frac{3K^2\omega_n}{R_L} \tag{4}$$

Battery load:

$$T_{r,n} = \frac{K^2\omega_n}{R_d + R_b} - \frac{V_{batt}K}{R_d + R_b} \tag{5}$$

Grid load:

$$T_{r,n} = (2.34K) \times \frac{2.34K\omega_n - V_d}{2R_{phase} + R_{over}} \tag{6}$$

$$V_d = \frac{1}{C_{WB}} \int \frac{V_{d0} - V_d}{2R_{phase} + R_{over}} - \frac{P}{\eta_{WB} V_d} \tag{7}$$

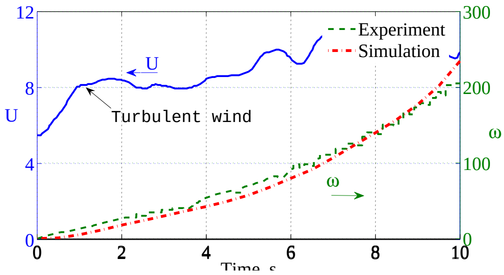

FIGURE 5. MEASURED AND PREDICTED ROTATIONAL SPEED DURING START-UP.

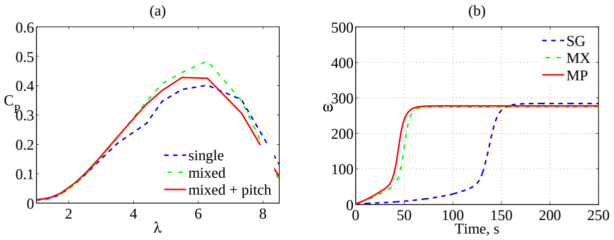

FIGURE 6. ROTOR PERFORMANCE: (a) POWER COEFFICIENTS AND (b) START-UP SEQUENCES UNDER STEADY WIND CONDITIONS.

where K is generator constant, R_L is load resistance, V_{batt} is battery voltage, R_d is generator resistance, R_b is battery resistance, R_{phase} is generator resistance per phase, R_{over} is overlap resistance, C_{WB} is grid converter capacitance, and η_{WB} is grid converter efficiency. A diagram of the model can be found in the appendix.

A validation of the MATLAB/SIMULINK model was performed by simulating the turbine tested by Wright and Wood [6]. In their experiment, a three-bladed, 2m diameter horizontal axis wind turbine was tested under turbulent wind. The turbine was designed to produce 600W at a rotor speed of 700RPM and a wind speed of 10 m/s. Figure 5 compares the measured data of Wright and Wood [6] with predicted rotational speed during start-up under the same turbulent wind conditions. It can be seen that they agree satisfactorily and provide confidence that the model captures the measured starting performance correctly.

RESULTS

ROTOR PERFORMANCE

Power coefficients of the three rotors used in this study (calculated from Blade Element Momentum theory (BEM)) and their starting sequences under a steady wind speed of 4 m/s calculated using the model described above are presented in Figure 6.

For the datum, single aerofoil case, it may be seen that a

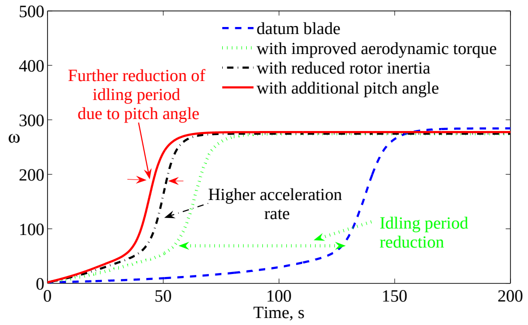

FIGURE 7. FACTORS CONTRIBUTING TO THE IMPROVED SELF-STARTING.

peak power coefficient occurred at a tip speed ratio of approximately six. The power coefficient curve of the mixed aerofoil blade is higher than that of single-blade for most tip speed ratios with a maximum of a twenty-percent increase in peak power coefficient at the same tip speed ratio. With the additional increment in pitch angle provided by the *MP* blade compared to the *SG* case there is a small increase in power coefficient at low tip speed ratios but a reduced peak power coefficient at higher tip speed ratios. The start-up curves demonstrate that the mixed aerofoil blades have a better starting performance under steady wind, roughly halving the starting time.

Figure 7 shows how this uplift in starting performance is achieved. Improvement of the blade aerodynamics leads to a reduced idling period. A further reduction of inertia will increase the rotor acceleration and hence shorten the acceleration period. Increase of pitch angle also further shortens the idling period but does not significantly affect the rotor acceleration.

Figure 8 presents time-dependent contributions of these effects (in percent) on the improved starting capability. These contributions were obtained by calculation of the change of rotational speed in Figure 7. The total change in rotational speeds between the datum and MP was first calculated then contribution of each factor was estimated. The latter calculation was performed by, for example, keeping pitch angle and moment of inertia constant whilst adding the mixed-aerofoil blade. Any difference would therefore solely be the effect of aerodynamics. Percent contributions of aerodynamic, inertia, and pitch angle were calculated by dividing the change of rotational speed caused by each factor by the total change. This calculation can be conceptually expressed as:

$$\Delta\omega_T = \Delta\omega_A + \Delta\omega_I + \Delta\omega_P \tag{8}$$

where $\Delta\omega_T$ is the total rotational speed improvement, $\Delta\omega_A$ is the rotational speed change due to aerodynamics, $\Delta\omega_I$ is the

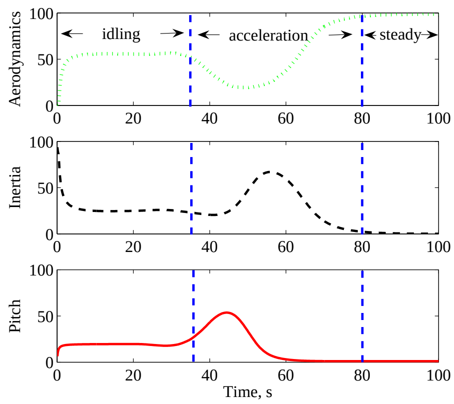

FIGURE 8. PERCENT OF CONTRIBUTIONS.

rotational speed change due to inertia, and $\Delta\omega_P$ is the rotational speed change due to pitch angle.

A percent of contribution (PC) of any improvement is then

$$PC_i = \frac{\Delta\omega_i}{\Delta\omega_T} \times 100 \tag{9}$$

where i denotes the appropriate abbreviation for A, I, and P (aerodynamics, inertia, and pitch improvements respectively).

It is apparent that the contribution of improved aerodynamics is low at the beginning and the main contributors for starting are the reduction of inertia and the increment in pitch angle that reduces the incidence angle experienced by the blade. After the rotor has spin, half of the improvement is provided by aerodynamic performance. The effects of pitch angle increment and reduced inertia appear again in the acceleration period and it appears that the reduction in inertia is the primary contributor in this region. The effects of inertia and pitch angle disappear when the rotor enters steady state (power-extraction performance under steady wind).

Although the *MP* blade had a lower peak power coefficient it gave the best starting characteristics. Since this was the main focus of the work, only comparisons between the *SG* and the *MP* are presented from here onwards.

SYSTEM PERFORMANCE

The effects of improved self-starting capability on the system performance are evaluated in two ways; time-varying behaviour (starting sequence) and Annual Energy Production (AEP). Starting sequences will be presented under real and simulated wind conditions. Predictions of AEPs are presented to evaluate the greater energy yield that can be obtained through the improvement of self-starting.

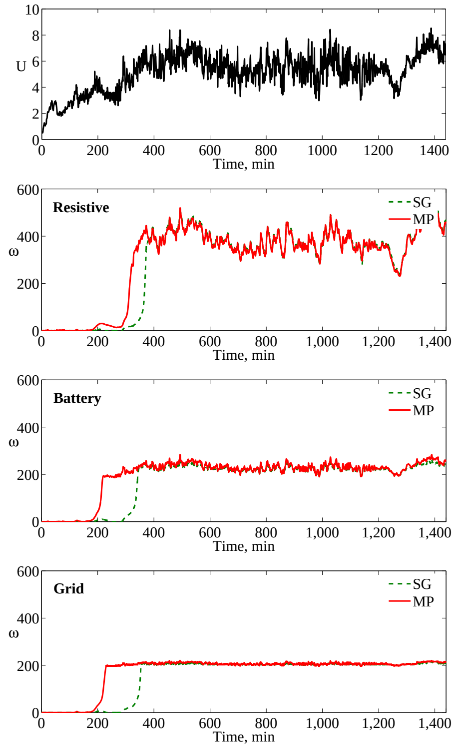

FIGURE 9. ONE DAY WIND VARIATION AND TURBINE ROTATIONAL SPEED FOR DIFFERENT LOADS.

Real turbulent wind variations In order to investigate the system performance in some detail for a reasonably long period of time, single day wind variations and turbine characteristics are shown in Fig. 9. To illustrate turbine performance under low wind speed conditions a day with relatively low wind speed was chosen from the measured data. For this day, the wind speed is lowest at the beginning of the day (1 m/s) but increases to around 6 m/s which is maintained with some fluctuation to the end of the day. The average wind speed is 5.135 m/s. Figure 9 also presents the corresponding rotor speeds for each of the three different load types and for the *SG* and *MX* cases.

For resistive heating, the difference between the *SG* and *MP* blades is narrower than those of battery and grid connection cases. This is because this type of load imposes resistive torque on the turbine as soon as the turbine spins. High fluctuation can also be seen in the energy-production period.

By way of contrast improvements in self-starting can be clearly seen for the battery-charging case. For the battery, resistive torque is not imposed on the turbine until the voltage generated by the turbine exceeds the battery voltage. With more torque generated by the modified blade and no resistive torque imposed by the battery, the modified turbine manages to rotate and reach the energy-production period more quickly than the original one, resulting in a shorter starting period and longer power-extraction period. In the power-extraction period, both turbines operate with nearly constant rotational speed of around 200rpm. The corresponding tip speed ratio under the average wind speed is approximately 5.0. At this tip speed ratio, it can be seen from the C_P curve (Fig. 6) that the *MP* turbine has a better performance and this is reflected in in a higher rotational speed during the power-extraction period. The same characteristics are seen in the grid connection case.

Simulated turbulent wind model In order to see the effect of improved self-starting at different sites simulated turbulent winds were used. These simulations provided two advantages over the real wind data: a more finely resolved time scale and the opportunity to explore different site characteristics. Two average wind speeds are explored (4 and 7 m/s) for a city centre terrain which is expected to have higher turbulence level. The turbulence level is normally expressed in terms of turbulent intensity factor (k_σ) and for this city centre terrain, this factor was approximated to be 0.434 [23]. It should be noted that the much smaller time interval between wind data samples required the use of a smaller overall simulation period in order to keep the output size manageable. Figures 10 and 11 present simulation results for twenty-minute periods.

Generally, it can be seen that the turbine behaviour is comparable to the real turbulent wind simulations. In the low wind simulations, the turbines begin to spin when there is a sudden increase in wind speed (or gust) from around two to five m/s that occurs at around 50 seconds into the simulation (Fig. 10). The modified blades manage to quickly capture the wind and accelerate themselves while the single blade suffers a longer idling period. Some useful energy is also produced in this region by the modified blades. After both blades have gone through the acceleration phase, it appears that they have comparable energy-production performance. The difference in starting behaviour between the two turbines is reduced when the average wind speed is higher as can be seen in Figure 11 (only battery case is presented).

Effects of loads on the turbine operating condition In order to compare and show deviations in turbine behaviour when connected to different loads, a norminalised rotational speed is plotted and presented in Figure 12.

The figure clearly shows that the loads have a significant influence on the system operational speed and if these loads are not considered, the operational speed will not reflect the real behaviour.

It is also observed that the system characteristic varies from load to load. For the resistive case, the operational speed increases linearly with wind speed and this often leads to a high fluctuation in rotational speed under turbulent wind, see Figure 9 for example. While the turbine connected to a battery exhibits

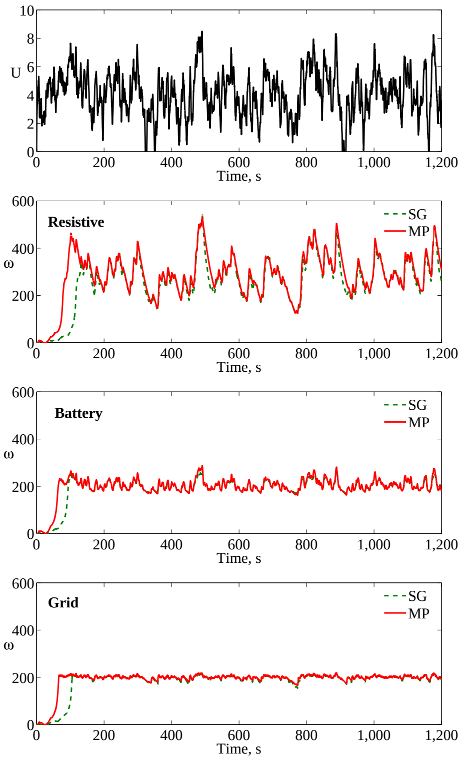

FIGURE 10. TURBINE ROTATIONAL SPEED AT AVERAGE WIND SPEED OF 4 m/s.

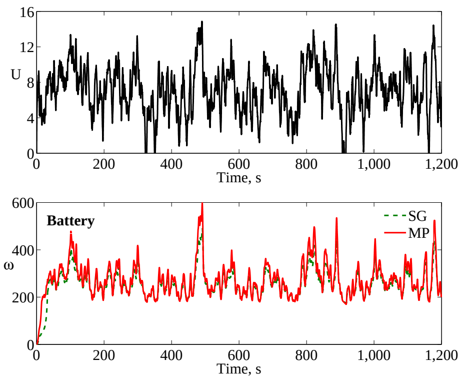

FIGURE 11. TURBINE ROTATIONAL SPEED AT AVERAGE WIND SPEED OF 7 m/s.

a moderate increase in rotational speed, the turbine connected to the grid exhibits a nearly constant rotational speed. The load characteristics, namely the voltage of the battery and the current control features of the grid converter [25] make them operate with a nearly constant rotational speed (Figure 9). One clear implication from this consideration is that if the load is not con-

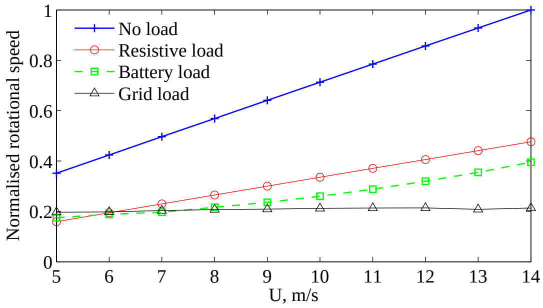

FIGURE 12. LOAD EFFECTS ON TURBINE ROTATIONAL SPEED.

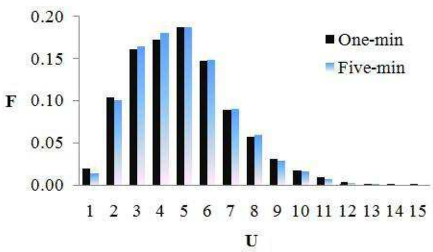

FIGURE 13. WIND DATA PROBABILITIES.

sidered, estimations of rotor speed and energy production will be misleading. Such estimations do not reflect the real improvement gained from the blade design.

ANNUAL ENERGY PRODUCTION (AEP)

In order to quantify the potential benefits of improved self-starting, energy production of the turbines was estimated using both the measured and simulated wind data.

Due to the lack of one-minute data over a year, energy production was calculated over one-month in order to evaluate the effect of different time intervals of measured wind data on the evaluation of improved starting on energy production.

One-minute and five-minute measured wind data have been processed to obtain probability distributions (Fig. 13). One-month energy productions for both data sets are listed in Table 3. Scale and shape factors (calculated by the maximum likelihood method [26]) are as follows: $c = 5.55$ and $k = 2.46$ for one-minute data and $c = 5.53$ and $k = 2.56$ for five-minute data. It appears that the two time intervals give nearly identical probabilities and energy productions indicating that they can be used interchangeably to evaluate effects on improved starting performance on energy yield prediction.

Further estimations on Annual Energy Production were performed using Weibull distribution functions. The AEP can be

TABLE 3. ENERGY PRODUCTION (kWh) AND NET ENERGY CHANGES (%).

Data set	Battery			Resist			Grid		
	SG	*MP*	%	*SG*	*MP*	%	*SG*	*MP*	%
One-min	78	91	17	35	37	5	152	201	32
five-min	76	89	17	34	36	6	150	200	33

TABLE 4. SITE PARAMETERS.

Sites	*c*	*k*
Low wind with low uniformity (LWL)	4.25	1.2
Low wind with high uniformity (LWH)	4.51	2.0
High wind with low uniformity (HWL)	10.62	1.2
High wind with high uniformity (HWH)	11.28	2.0

calculated from:

$$AEP = 8760 \sum_{V_{start}}^{V_{stop}} P(v_i)F(v_i) \tag{10}$$

where V_{start} is the cut-in wind speed, V_{stop} is the cut-out wind speed, P is power produced by the turbine at a specific wind speed, and F is Weibull distribution function. The Weibull distribution of any wind variation at a site can be expressed in the form

$$F = (\frac{k}{c})(\frac{v}{c})^{k-1} \exp[-(\frac{v}{c})^k] \tag{11}$$

where v is wind speed, c is a scale factor (m/s), and k is a shape factor. The scale and shape factors are site-specific and are related to each other as follows:

$$v = c\Gamma(1+\frac{1}{k}) \tag{12}$$

where Γ is the gamma function. It can be seen that the value of c is proportional to the average wind speed and it can be interpreted as a characteristic speed of the site while the k factor defines the uniformity of the wind and, hence, the shape of distribution. The site parameters used in this estimation are defined and tabulated in Table 4.

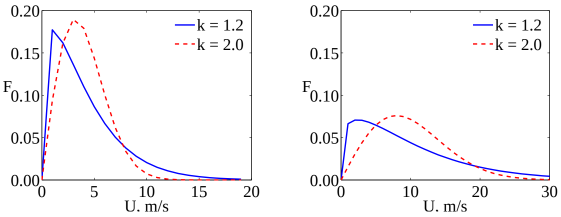

FIGURE 14. WEIBULL DISTRIBUTIONS.

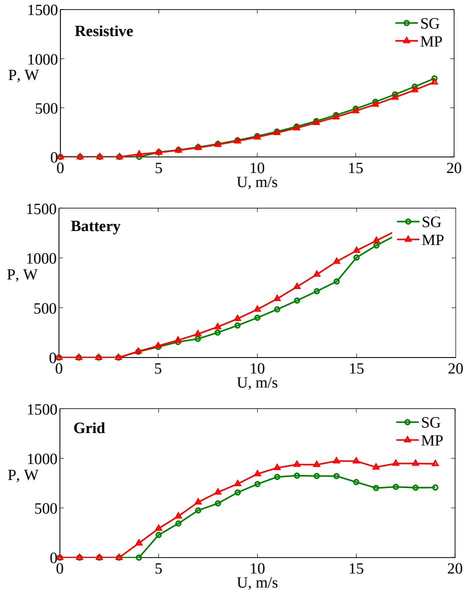

FIGURE 15. POWER CURVES: BATTERY CHARGING, RESISTIVE HEATING, AND GRID CONNECTION.

The first two Weibull distributions are defined to represent low wind speeds (4 m/s) at different sites having different wind distribution ($k = 1.2$ and $k = 2.0$). The others are defined to represent higher wind speed (10 m/s) at the same sites. The cut-out wind speed is assumed to be 20 m/s for all turbines. The Weibull distributions are presented in Figure 14. Power curves of the turbines connected to different loads are shown in Figure 15. From the wind distributions and the power curves, the energy captured over a year was evaluated assuming that there would be no outages for planned or unplanned maintenance. Table 5 lists AEPs and net energy changes of all cases.

For resistive heating, the two curves are nearly the same. An improvement from the modification of the blade from single to mixed-blade design is only seen at the low wind speed of 4 m/s and is very small. The power generated by the modified blade is very slightly lower than the original at higher wind speeds. This is mainly because of the resistive torque that is exerted on the

TABLE 5. ANNUAL ENERGY PRODUCTION (kWh) AND NET ENERGY CHANGES (%).

Case	Battery			Resist			Grid		
	SG	*MP*	%	*SG*	*MP*	%	*SG*	*MP*	%
LWL	846	993	17	404	412	2	1403	1807	29
LWH	630	727	15	264	294	12	1181	1657	40
HWL	245	280	14	1261	1219	-3	2988	3657	22
HWH	351	405	16	1822	1751	-4	4393	5287	20

turbine by the load. In resistive heating, this resistive torque will act on the turbine as soon as the turbine spins and continuously increases with rotational speed. At high rotational speed, the modified blade will not produce as high a torque as the original because the blade at the root will stall and this results in a smaller net torque and a modest reduction in energy production.

For the battery case, both blades begin to produce useful power at 4 m/s but the modified blade produces higher power for all wind speeds. The most significant improvement is found in the grid connection case. The modified version outperforms the original one for all wind speeds.

Generally, it can be seen that increases are found for most cases using the modified blade geometry except the resistive load at high wind speed. Comparisons of net changes in energy production using measured wind data and simulated Weibull distributions show that they are in the same order. Though of course the high temporal resolution model provides a means of actually physically realising changes in power curves via aerodynamic designs.

CONCLUSIONS

The effects of improved starting capability of small HAWTs on energy production when connected to different loads under both real and simulated wind variations have been investigated. The following conclusions are made:

1. This paper has used aerofoil data at the correct Reynolds number and covering the very high angles of attack experienced at startup.
2. This paper includes the effect of load types on turbine startup performance.
3. An improvement in self-starting has been achieved through the exploitation of a “mixed-aerofoil” blade. Both aerodynamic improvements and a reduction in inertia are obtained by the use of such a mixed-aerofoil blade.
4. Improving the start up performance can improve the energy yield of the device by up to 40%.
5. The improvement in energy yield is greatly dependent on

the wind turbine load. Although significant increases were found for battery charging and grid connection under resistive heating the energy yield could actually decline by up to 4% when improved self-starting was implemented.

6. The starting capability and load types to which they are connected to should be considered along with the peak power-extraction scheme in the design process.

ACKNOWLEDGMENT

The authors are grateful to Professor David Wood at University of Newcastle, Australia for providing valuable data. The authors also acknowledge the help of David Hails at NaREC (National Renewable Energy Centre) for providing us with their wind data. The authors would like to thank Dr. Jim Bumby and Dr. Nick Stannard for suggestions and allowing us to use their wind model.

REFERENCES

[1] DTI, 2003. Energy White Paper in Our energy future - creating a low carbon economy. Tech. rep., DTI.

[2] Fuglsang, P., and Madsen, H., 1999. “Optimisation Method for Wind Turbine Rotors”. *Wind Engineering and Industrial Aerodynamics*, ***80***, pp. 191–206.

[3] Lanzafame, R., and Messina, M., 2009. “Optimal Wind Turbine Design to Maximize Energy Production”. *Proc. IMechE. J. Power and Energy*, ***222***, pp. 93–101.

[4] Ebert, P., and Wood, D., 1997. “Observations of the Starting Behaviour of a Small Horizontal-axis Wind Turbine”. *Renewable Energy*, ***12***, pp. 245–257.

[5] Mayer, C., Bechly, M., Hampsey, M., and Wood, D., 2001. “The Starting Behaviour of a Small Horizontal-axis Wind Turbine”. *Journal of Renewable Energy*, ***22***, pp. 411–417.

[6] Wright, A., and Wood, D., 2004. “The Starting and Low Wind Speed Behaviour of a Small Horizontal Axis Wind Turbine”. *Journal of Wind Engineering and Industrial Aerodynamics*, ***92***, pp. 1265–1279.

[7] Hampsey, M., 2002. “Multi-objective Evolutionary Optimisation of Small Wind Turbine Blades”. PhD thesis, School of Engineering, University of Newcastle.

[8] Wood, D., 2004. “Dual Purpose Design of Small Wind Turbine Blades”. *Journal of Wind Engineering*, ***28(5)***, pp. 511–527.

[9] Clifton-Smith, M., and Wood, D., 2007. “Further Dual Purpose Evolutionary Optimization of Small Wind Turbine Blades”. *Journal of Physics: Conference Series 75*.

[10] Tangler, J., and Somers, D., 1995. NREL Airfoil Families for HAWTs. Tech. Rep. NREL/TP-442-7109, National Renewable Energy Laboratory, January.

[11] Giguere, P., and Selig, M., 1998. “New Airfoils for Small Horizontal Axis Wind Turbines”. *ASME Journal of Solar Energy Engineering*, ***120***, pp. 108–114.

[12] NWTC, 2003. Wind Turbine Generator System Power Performance Test Report for the Bergey Excel-S/60 Wind Turbine with BW03 Airfoil Blades. Tech. Rep. NREL/EL-500-33450.

[13] NWTC, 2003. Wind Turbine Generator System Power Performance Test Report for the Bergey Excel-S/60 Wind Turbine with SH3052 Airfoil Blades. Tech. Rep. NREL/EL-500-33452.

[14] Burton, T., Sharpe, D., Jenkins, N., and Bossanyi, E., 2001. *Wind Energy Handbook*. John Wiley & Sons Ltd.

[15] Selig, M., 2003. Low Reynolds Number Airfoil Design. Lecture notes, The von Karman Institute for Fluid Dynamics, November.

[16] Selig, M., 1997. Summary of Low-speed Airfoil Data. Tech. rep., SoarTech Publication.

[17] Worasinchai, S., Ingram, G., and Dominy, R., 2010. “A Low-Reynolds-number, High-Angle-of-Attack Investigation of Wind Turbine Aerofoils”. *To be published*.

[18] Muljadi, E., and Green, J., 2002. Cogging Torque Reduction in a Permanent Magnet Wind Turbine Generator. Tech. Rep. NREL/CP-500-30768, National Renewable Energy Laboratory.

[19] Bumby, J., Stannard, N., and Martin, R., 2006. “A Permanent Magnet Generator for Small Scale Wind Turbines”. In Proceedings of the 17th International Conference on Electrical Machines.

[20] Lu, K., Rasmussen, P., and Ritchie, E., 2006. “An Analytical Equation for Cogging Torque Calculation in Permanent Magnet Motors”. In Proceedings of the 17th International Conference on Electrical Machines.

[21] Miwa, M., and Dibben, D., 2004. “High Accuracy Torque Calculation for a Rotating Machine Using Adaptive Meshing”. *IEEE Transactions on Magnetic*.

[22] Berges, B., 2007. “Development of Small Wind Turbines”. Master’s thesis, Department of Mechanical Engineering, Technical University of Denmark.

[23] Stannard, N., 2008. “Generator Design for, and Modelling of, Small-scale Wind Turbines”. PhD thesis, School of Engineering, University of Durham.

[24] Hails, D., 2010. Private communication.

[25] Bumby, J., 2010. Lecture notes. Small Scale Wind Turbines.

[26] Seguro, J., and Lambert, T., 2000. “Modern Estimations of the Parameters of the Weibull Wind Speed Distribution for Wind Energy Analysis”. *Journal of Wind Engineering and Industrial Aerodynamics*, ***85(1)***, pp. 75–84.

Appendix A: MATLAB/Simulink modelling

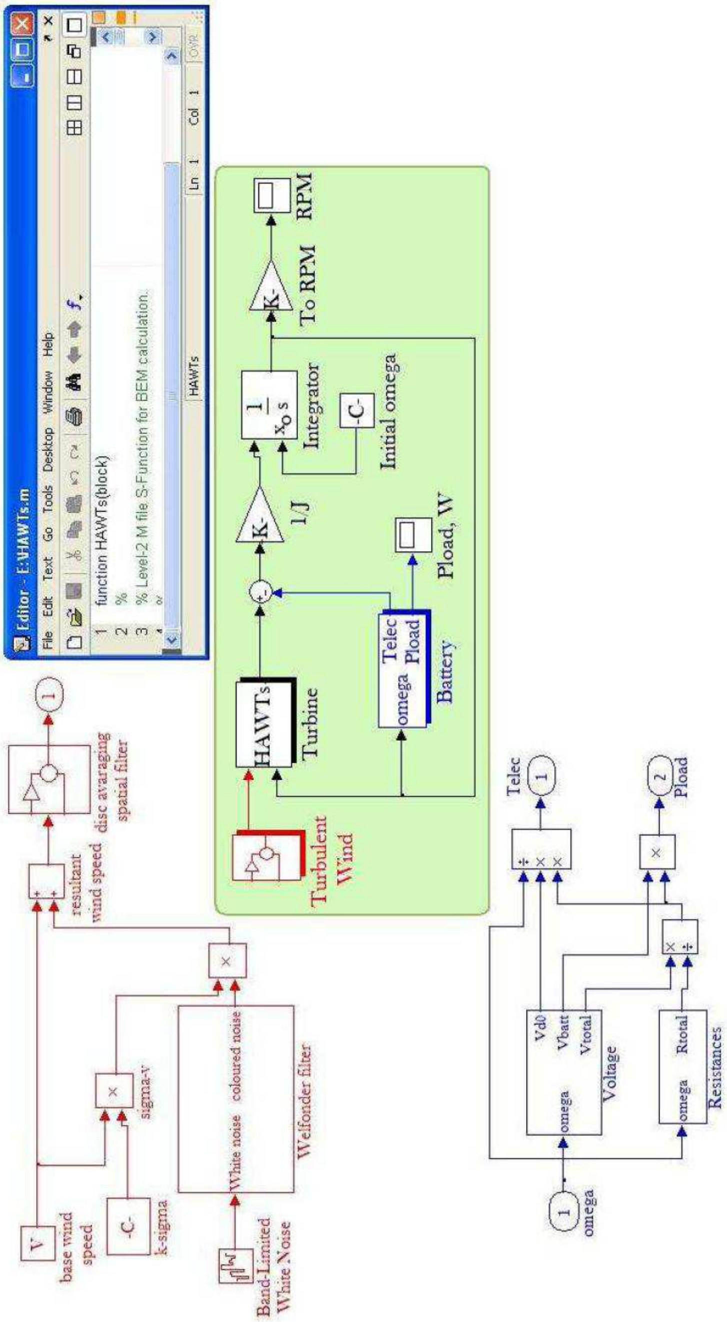

FIGURE 16. Simulink modelling.